to appear in Journ. Appl. Phys. (with minor changes) 906

Structural and optical properties of annealed proton-exchanged waveguides in *z*-cut $LiTaO_3$

H. Åhlfeldt,

Department of Physics II, Royal Institute of Technology, S-100 44 Stockholm, Sweden.

TEL: +46 8 790 7317, FAX: +46 8 789 6672

J. Webjörn,

Optoelectronics Research Centre, Univerity of Southampton, Hants SO9 5NH, UK

P. A. Thomas and S. J. Teat,

University of Warwick, Coventry CV4 7AL, Warwick, UK

ABSTRACT

The structural properties of annealed proton-exchanged waveguides in *z*-cut $LiTaO_3$ have been investigated. Observations made in a polarizing microscope together with infrared absorption measurements indicate the formation of monoclinic phase $Li_{(1-x)}H_xTaO_3$ after proton exchange in pure pyrophosphoric acid. This monoclinic phase disappears after weak annealing. Characterization using high-resolution X-ray diffraction shows that the *c* lattice parameter is 0.57% larger in the exchanged layer than in the bulk. On annealing the *c* parameter relaxes and in addition there appears a second diffraction peak in the X-ray rocking curves. This peak is attributed to α-phase $Li_{(1-x)}H_xTaO_3$. A model for the increase of the refractive index is suggested

where the main reason for the difference in index increase between proton-exchanged waveguides in $LiTaO_3$ and $LiNbO_3$ is the larger value of the spontaneous polarization of $LiNbO_3$. The model predicts an increase of the refractive index on annealing of $LiTaO_3$ which is of the same order of magnitude as that experimentally observed. The short-term post-annealing index decrease observed in a previous study is further examined and suggested to be closely related to the ferroelectric domain reversal.

I. INTRODUCTION

Proton-exchanged waveguides in $LiTaO_3$ are of great interest for efficient second-harmonic generation [1]. Quasi-phase-matched waveguides fabricated through annealed proton exchange in $LiTaO_3$ may be used in combination with infrared diode lasers to realize compact coherent blue light sources for *e.g.* optical data storage. In the same manner as it does in $LiNbO_3$, proton exchange in $LiTaO_3$ leads to an increase of the extraordinary refractive index (n_e) and a decrease of the ordinary refractive index (n_o). However, some of the optical properties exhibit significant differences; the increase of the extraordinary index is smaller in $LiTaO_3$ ($\Delta n_e \approx 0.012$) than in $LiNbO_3$ ($\Delta n_e \approx 0.12$), the index initially increases on annealing in $LiTaO_3$ [2,3,4] and waveguides in $LiTaO_3$ are unstable even after post-exchange annealing [4,5,6]. In this study we use optical characterization methods and high-resolution X-ray diffraction (HRXRD) to investigate some basic properties of annealed proton-exchanged waveguides in $LiTaO_3$ and try to explain some of the differences between these waveguides and the more thoroughly investigated waveguides in $LiNbO_3$.

In Sec.II we describe the preparation of the waveguides investigated in the study. In Sec.III we present the results of observations made in the polarizing microscope and in Sec.IV we discuss those results in connection with observations made during infrared (IR) absorption measurements. The results of HRXRD characterization are described and discussed in Sec.V and in Sec.VI a model for the refractive-index change in ferroelectric materials is used to explain the difference of the index increase in $LiNbO_3$ and $LiTaO_3$. The drastic short-term index changes in certain $LiTaO_3$ waveguides, reported in a previous study [4], are discussed in Sec.VII and a possible explanation is proposed. Sec.VIII summarizes this study.

II. SAMPLE PREPARATION

Proton-exchanged waveguides were fabricated by immersion of *z*-cut $LiTaO_3$ samples in pyrophosphoric acid in a platinum beaker. New acid was used each time. Subsequent annealing was carried out in air in a horizontal tube furnace.

Samples with a range of hydrogen concentrations were also obtained through proton exchange in a eutectic mixture of $ZnSO_4$, K_2SO_4 and Na_2SO_4 [7] with an addition of $KHSO_4$ to control the hydrogen concentration in the melt. This melt was proposed and used by Ganshin *et al.* [8], and in a previous study [4] we have used it to investigate the concentration dependence of the refractive index of proton exchanged $LiTaO_3$ waveguides. The $KHSO_4$ molality, C_M, in the salt melt was varied between 0.015 and 0.12 mol/kg. The *z*-cut $LiTaO_3$ samples were immersed in the melt for 2 h at 400°C.

III. OBSERVATIONS IN THE POLARIZING MICROSCOPE

Z-cut samples were studied in a polarizing microscope with the light propagating along the crystal *z* axis, *i.e.* ordinarily polarized light. As expected, no light came through when an untreated uniaxial sample was placed between the polarizer and the crossed analyser.

Figure 1 is a micrograph of the *z* face of a proton-exchanged $LiTaO_3$ sample viewed in the polarizing microscope. The sample has been exchanged for 5 h at 290°C. In this case one sees a mosaic of biaxial domains. The black regions correspond to domains extinguishing at the present angle of rotation of the sample. When the sample is rotated around the *z* axis different domains extinguish at angles 30° apart. We believe that the domains are regions of a biaxial monoclinic phase $Li_{(1-x)}H_xTaO_3$ in three orientations. Close inspection revealed that there were three distinct optically-biaxial domain orientations with axes rotated by 120° with respect to each other. Now, $LiTaO_3$ is described by point group 3m which is of order 6. The existence of

three orientational states is consistent with a lowering of symmetry to a monoclinic point group of order 2 in the hydrogen-containing phase. Similar domain patterns were also observed in samples exchanged at 260°C and 220°C. However, we saw no such pattern in as-exchanged *z*-cut $LiNbO_3$ samples. Nor did we observe any biaxial domains in the $LiTaO_3$ sample exchanged in the 0.12 mol/kg sulphate-salt melt, *i.e.* the melt with the highest molality used in our study.

One $LiTaO_3$ sample exchanged at 260°C for 6 h was annealed for 10 min at subsequently higher temperatures; 100, 150, 200, 250 and 300°C. After each heat treatment the sample was cooled to room temperature and examined in the polarizing microscope. The domains were still present after heating to 250°C but disappeared after the heat treatment at 300°C.

IV. INFRARED ABSORPTION MEASUREMENTS

As-exchanged $LiTaO_3$ and $LiNbO_3$ exhibit two characteristic IR absorption peaks; one sharp peak at 3500 cm^{-1} polarized perpendicular to the crystal *z* axis and one broad unpolarized peak at 3250 cm^{-1}. The unpolarized 3250 cm^{-1} peak is much less pronounced in *z*-cut samples than in *x*-cut samples [9,10] and has been shown to be due to a thin surface layer [9,11,12].

IR absorption measurements were carried out in a Perkin Elmer FTIR spectrophotometer. Since the light was polarized perpendicular to the crystal *z* axis (*z*-cut samples) both absorption peaks were detected. Figure 2 shows the IR transmission spectra for three different samples all initially exchanged for 5 h at 260°C; (a) as-exchanged, (b) annealed for 10 min at 300°C, and (c) annealed for 15 min at 350°C. It is clear that the 3250 cm^{-1} peak disappears in the very initial stage of the annealing. We also measured the IR spectrum for the sample exchanged in the 0.12 mol/kg sulphate-salt melt for 2 h at 400°C. The absorption at 3500 cm^{-1} was in that case very strong due to a large amount of hydrogen in the sample but no distinct peak at 3250 cm^{-1} was observed. A

$LiNbO_3$ sample exchanged for 5 h at 260°C was also characterized. Nor in this case did we observe a distinct peak at 3250 cm^{-1}, though in agreement with earlier studies [10,13] we observed a broad shoulder extending from the main 3500 cm^{-1} band to lower wavenumbers.

We attribute the 3250 cm^{-1} peak in the IR absorption spectrum to the layer of monoclinic $Li_{(1-x)}H_xTaO_3$ revealed by the extinctions observed in the polarizing microscope (*cf.* Sec.III). The presence of a monoclinic phase $Li_{(1-x)}H_xTaO_3$ is also supported by a comparison of the IR spectrum obtained here with the IR spectrum for monoclinic phase $Li_{(1-x)}H_xNbO_3$ powder presented in Ref.14. The presence of a monoclinic layer in as-exchanged *z*-cut $LiNbO_3$ was recently proposed by Ziling *et al.* [13]. In another study biaxial layers were found to form in *x*- and *y*-cut $LiNbO_3$ but not in *z*-cut $LiNbO_3$ [15]. As mentioned in the previous section we have not observed any biaxial domains in our as-exchanged $LiNbO_3$ samples.

Though no pure monoclinic phase $Li_{(1-x)}H_xNbO_3$ seems to form in *z*-cut $LiNbO_3$ the broad shoulder in the IR spectrum suggests the existence of hydrogen atoms that do not directly substitute for lithium atoms in the structure. It has been suggested that this unpolarized absorption band is due to the presence of a thin layer of cubic phase $HNbO_3$ [11]. X-ray diffraction from congruent $LiNbO_3$ powders has shown that for $x > 0.77$, rhombohedral $Li_{(1-x)}H_xNbO_3$ coexists with cubic $HNbO_3$ [14]. For *z*-cut single-crystal $LiNbO_3$ the situation is less clear. Canali *et al.* [16] were unable to detect any new structure whereas Ito and Kawamoto [17] observed an X-ray Bragg reflection which agreed with a reflection from cubic phase $HNbO_3$.

The disappearance of the biaxial domains and the 3250 cm^{-1} peak in the very initial stage of the annealing suggests that the phase transformation from monoclinic to rhombohedral $Li_{(1-x)}H_xTaO_3$ cannot be the cause of the increase of the refractive index on annealing which occurs in $LiTaO_3$ waveguides. This index increase is observed to continue for much longer annealing times (*cf.* Fig.3). Previously, Tada *et al.* have connected the index increase on annealing and the disappearance of the 3250 cm^{-1} absorption peak with the migration of protons from interstitial to

substitutional sites in the structure [2]. By contrast however, we have observed that the 3250 cm^{-1} peak disappears too soon in the ordering process to be associated with the increase of the refractive index.

V. HIGH-RESOLUTION X-RAY DIFFRACTION

Alternatives to the theory that a change of site preference of the protons is responsible for the index change seen on annealing are that the index change is caused by crystal phase transitions or that large changes of the lattice parameters lead to a volume effect. Phase transitions could also explain the post-annealing index changes observed in a previous study [4]. To investigate the effect of lattice-parameter changes and possible phase transitions on the optical properties of the waveguides, HRXRD measurements were carried out on some of the waveguides which were optically characterized in the foregoing study.

A. HRXRD:Experimental

The HRXRD measurements were carried out on a Philips Materials Research Diffractometer. The CuK_α radiation was selected using a Bartels monochromator consisting of four germanium crystals set for 2 2 0 reflections for λ=1.5406 Å. X-ray rocking curves (XRC) (scans as function of ω-2θ with a slit having a 2θ acceptance angle of 2° at the detector) for the 0 0 6 and 0 0 12 reflections, and for some deep waveguides also the 0 2 16 reflection, were recorded to determine the relative change of the *c* lattice parameter ($\Delta c/c$) in the hydrogen-diffused region.

Figure 4(a) shows the XRC for the 0 0 6 reflection from samples exchanged for 5 h at 260°C; one as-exchanged sample (A) and one annealed for 5 min at 350°C (B). The difference in the Bragg angle θ for the high-angle substrate peak and the low-angle waveguide peak for the

as-exchanged sample corresponds to a $\Delta c/c$ of 0.58 %. The same $\Delta c/c$ value was obtained for a sample exchanged for 1 h at 260°C and for a sample exchanged for 12 h at 220°C. This value is also in good agreement with the value 0.57 % reported in Ref.2.

The large widths of the XRC for the as-exchanged sample suggests that the crystal structure has been severly distorted by the proton exchange. Annealing for 5 min improves the crystal quality and causes a relaxation of the *c* parameter; the low-angle waveguide peak sharpens and moves towards the substrate peak (Fig.4(a):B). Figure 4(b) shows the XRC for the 0 0 12 reflection for samples exchanged for 5 h at 260°C and then annealed at 350°C for 10 min (C), 20 min (D), 1 h (E), and 4 h (F). A third broad peak appears between the substrate peak and the proton-exchange peak. This peak was observed also by Tada *et al.* [2] and was attributed to the formation of a new crystal phase in the exchanged layer. As the annealing proceeds the two satellite peaks move towards the substrate peak. After 4 h annealing the middle peak has more or less merged with the low-angle peak and appears as a shoulder on that peak. For longer annealing times the hydrogen-diffused region becomes quite thick. The reflection from the substrate hence becomes weak and is difficult to resolve from the reflection from the diffused region. The change of the *c* parameter for long annealing times is therefore more approximately estimated.

Figure 5 shows $\Delta c/c$ as function of root of annealing time for the samples exchanged for 5 h at 260°C and then annealed at 350°C for different periods of time. $\Delta c/c$ changes from 0.58 % in the as-exchanged sample to approximately 0.1 % in a sample exchanged for 16 h. There is a strong relaxation of the *c* parameter during the first hour of annealing.

The change of the *c* parameter was measured also for the waveguides fabricated by proton exchange in sulphate-salt melts. The XRC for these samples were similar to those for the annealed

samples. Figure 6 shows $\Delta c/c$ versus $KHSO_4$ concentration. The change of the c parameter increases with increasing $KHSO_4$ concentration and for 0.12 mol/kg $\Delta c/c$ is approximately the same as for the as-exchanged samples discussed above.

A $LiNbO_3$ sample exchanged for 5 h at 260°C was also characterized. The XRC for the 0 0 6 reflection is shown in Fig.7. In this case $\Delta c/c$ is 0.32 % for the largest proton-exchange peak and approximately 0.46 % for the smaller low-angle peak. This seems to be in good agreement with the results obtained by Minakata *et al.* [18] for waveguides exchanged in benzoic acid at 220°C for 6 h. Though that study indicated that the c parameter may be somewhat dependent on the exchange conditions (for 105 h exchange at 245°C the largest proton-exchange peak is shifted to $\Delta c/c = 0.46$ %) it is quite clear that the change of the c parameter is greater in $LiTaO_3$ than in $LiNbO_3$.

To determine the relative change of the a lattice parameter ($\Delta a/a$) it is necessary to determine the spacing between the lattice planes for an asymmetric reflection with an a-parameter contribution. In the case of asymmetric reflections, a nonuniform deformation of the lattice parameters ($\Delta a/a \neq \Delta c/c$) will lead to a change of the spacing of the lattice planes as well as a change of the angle between the lattice planes and the surface of the sample. Both these effects contribute to a shift of the angle of reflection for a XRC peak. A convenient way to separate the two contributions and to obtain the difference in lattice-plane spacing between the bulk and the exchanged layer is to record two-dimensional diffraction space maps of particular reflections. This requires the use of the analyzer crystal to reduce the acceptance angle at the detector to 12 arcseconds in 2θ. Using the diffractometer in this triple-axis configuration ω *vs.* ω-2θ maps of the 5 0 8 and 4 0 10 reflections were recorded.

Figure 8 shows the diffraction space map of the 5 0 8 reflection for a sample exchanged for 5 h at 260°C and then annealed for 10 min at 350°C. The peak in the top-right corner is the substrate peak and the peak in the bottom-left corner is the peak from the exchanged layer. The calculated

change of the spacing of the (5 0 8) lattice planes is 0.085 %. From the above measurement of $\Delta c/c$ (0.42 % after 10 min annealing), a $\Delta a/a$ of -0.03 % was calculated. Diffraction space maps were recorded also for some other samples. The magnitude of $\Delta a/a$ was found to decrease from 0.05 % in an as-exchanged sample to 0.01 % in a sample annealed for 1 h. In all cases $\Delta a/a$ was negative. The small magnitude of $\Delta a/a$, which is very different from the results of $LiNbO_3$ powder experiments [14], is reasonable since the expansion in the *xy* plane is constrained by the bulk lattice.

B. HRXRD:Discussion

In the interpretation the HRXRD experiments we must account for the fact that we see a response which is integrated over the depth of the sample. A graded concentration profile will broaden an XRC because of the existence of a range of different lattice parameters. It is only for a step profile that we can expect two sharp peaks, one for the layer and one for the substrate.

In Fig.4(b) we saw that during annealing there appears a new peak for a smaller $\Delta c/c$ than the initial proton exchange layer. With longer annealing the two peaks move towards the substrate value of *c*. Figure 5 shows the $\Delta c/c$ values for the two peaks as function of annealing time. In the following we propose an explanation for these observations.

We assume that the phase diagram of $Li_{(1-x)}H_xTaO_3$ is similar to that of $Li_{(1-x)}H_xNbO_3$ derived from powder experiments [14]: For $x < x_\alpha$ the crystal remains in α phase, for $x > x_\beta$ the crystal is in β phase, and for $x_\alpha < x < x_\beta$ the crystal is composed of a mixture of the two phases. After raw proton exchange, during which approximately 80 % of the lithium is substituted for hydrogen [3], we have a layer of pure β phase $Li_{0.2}H_{0.8}TaO_3$. During annealing there appears a region with intermixed small grains of α and β phase. In this stage it is known that the losses of the waveguide become very high due to scattering [19]. The volume of β phase then decreases until after long

annealing the waveguide is completely in the α phase. It is reasonable to assume that the two satellite diffraction peaks in Fig.4(b) correspond to α- and β-phase $Li_{(1-x)}H_xTaO_3$, respectively. The continuous movement of both peaks towards the substrate peak can be explained by the interaction of the two phases in the mixed α+β region. The small grains are strained by the surrounding crystal and therefore $\Delta c/c$ of both α- and β-phase grains changes when the volume ratio between α and β phase changes. For x values near the boundary between pure α phase and mixed α+β phase, *i.e.* $x \approx x_\alpha$, the α phase dominates and $\Delta c/c$ for the α phase changes continuously. Near x_β the β phase dominates and $\Delta c/c$ for the β phase changes continuously. The interaction between the α and β phases explains why we observe two diffraction peaks which move together towards the substrate peak. If the two phases did not strain each other we would rather observe the transformation of β-phase $Li_{(1-x)}H_xTaO_3$, with the value of c equal to the value at $x = x_\beta$, to α-phase $Li_{(1-x)}H_xTaO_3$, with the value of c equal to the value at $x = x_\alpha$. The α-phase peak would not shift until all the β phase has been transformed into the α phase. Diffusion would thereafter lower the hydrogen concentration in the α phase and lead to a relaxation of the c parameter.

Though the large relaxation of the c parameter during the first period of annealing may contribute to the increase of the refractive index on annealing of $LiTaO_3$, the HRXRD measurements did not reveal any unexpected crystal phase or anomalous behaviour which alone can explain why $LiTaO_3$ behaves differently from $LiNbO_3$.

VI. INDEX-INCREASE MECHANISM

The change of the refractive index in proton-exchanged $LiTaO_3$ and $LiNbO_3$ can be estimated by considering four different contributions to the index change: (i)Δn^P due to a change of the spontaneous polarization P_S, (ii) Δn^α due to a difference in the molar polarization α_M of Li_2O and H_2O, (iii) Δn^V due to a change of the volume of the unit cell, and (iv) Δn^ε induced by the

elastooptic effect. Versions of this model have been used to estimate the index change in titanium-diffused [20] and proton-exchanged [21,13] $LiNbO_3$ and proton-exchanged $LiTaO_3$ [22,23].

To calculate Δn^P it is necessary to estimate the value of P_S in the exchanged region. This is discussed in the first part of this section. Thereafter, we use the refractive-index model to estimate, first the index increase in as-exchanged $LiTaO_3$ and $LiNbO_3$, and then the index changes on annealing.

A. Spontaneous polarization of $Li_{(1-x)}H_xTaO_3$

The principal origin of P_S in $LiTaO_3$ and $LiNbO_3$ is the ordered displacement of the Li ions in the $+c$ direction from the oxygen planes together with the induced distortion of the Ta/Nb ions from the centres of the oxygen octahedra. The bulk spontaneous polarization $P_{S,0}$ is 0.71 $C \cdot cm^{-2}$ for $LiNbO_3$ and 0.50 $C \cdot cm^{-2}$ for $LiTaO_3$ [24]. The value of P_S after proton exchange, $P_{S,PE}$, is not known through direct measurements. Here, we discuss a model which is consistent with recent nonlinear-susceptibility measurements.

The polarization of the 3500 cm^{-1} peak in the IR absorption spectrum suggests that during the proton exchange process the protons take positions within the oxygen planes rather than simply occupying the Li sites. In Refs.21 and 22, the reduction of P_S after proton exchange was assumed to be the result exclusively of the reduction of the contribution from the Li ions. However, the post-exchange reduction of the electrooptic [2,18,25] and nonlinear-optic [26,27,28,29] coefficients, the values of which mainly depend on the polarizabilities of the Ta/Nb-O bonds [30], indicates that the exchange process also relaxes the distortion of the Ta/Nb ions from the centres of the oxygen octahedra. This is also supported by the similarity between the Raman spectra for proton-exchanged $LiTaO_3$ and paraelectric phase $LiTaO_3$ [31].

If the substitution of a proton for a Li ion is essentially assumed to result in a relaxation of the nearest neighbour Ta ion to the center of its surrounding O_6 octhahedron, the reduction of P_S in $Li_{(1-x)}H_xTaO_3$ will be proportional to x, so that

$$P_{S,PE} = (1-x)P_{S,0} \tag{1}$$

However, this model is not consistent with the observations in Refs.27 and 29 which indicate that the nonlinear-optic coefficient d_{33} is approximately zero even for rather low hydrogen concentrations, $x = 0.3$ - 0.5 according to Ref.29. Di Domenico and Wemple [32] have shown that the electrooptic and nonlinear-optic coefficients of oxygen-octahedra ferroelectrics can be linearly related to P_S. Thus, the observed reduction of d_{33} implies that also $P_{S,PE}$ should also be approximately zero for $x = 0.3$ - 0.5, which is not in agreement with Eq.(1).

A model in which the reduction of P_S is proportional to x seems reasonable only if we consider an artificial situation where a fraction x of the Li ions, at sites corresponding to a uniform polarization, are simply substituted by protons taking nonpolar sites. This, however, is not the relevant physical situation. The equilibrium crystal structure is attained when the crystal is cooled to room-temperature after a period of high-temperature (>300°C) annealing during which diffusion of Li ions and protons in opposite directions takes place. When the temperature is decreased the diffusing ions will come to rest at equilibrium sites in the crystal structure. As stated above, the protons take positions within the oxygen layers whereas the Li ions can take positions at either side of the oxygen plane (corresponding to dipole moments with different signs). When the hydrogen concentration is low enough it seems reasonable that the position of Li ions is determined by the orientation of the undisturbed bulk below. This is supported by experiments with proton-exchange in domain-inverted $LiNbO_3$ samples which show that during annealing there takes place a regrowth of material whose ferroelectric orientation depends on the orientation of the substrate below [33]. From a comparison with experiments in Ref.19 the

concentration limit for regrowth was found to correspond fairly well with the estimated maximum concentration for the α phase. For high proton concentrations ($x > x_\beta$), it is possible that the influnce of the substrate polarization is disturbed so that such an epitaxial regrowth of material with homogeneous ferroelectric orientation does not take place. If the Li ions instead take positions on either side of the oxygen layer with equal probability, this implies zero net P_S in the exchanged region.

Finally the following model for $P_{S,PE}$ is proposed: For $x > x_\beta$ we have an unpolarized β phase with $P_{S,PE} = 0$. For $x < x_\alpha$ we have a polarized α phase. It seems reasonable that the linear model described by Eq.(1) should hold for the α phase. For $x_\alpha < x < x_\beta$ we have a mixed α+β phase where P_S decreases linearly from $(1\text{-}x_\alpha)P_S$ at x_α to zero at x_β.

B. As-exchanged waveguides

(i) In the ferroelectric phase of $LiNbO_3$ and $LiTaO_3$, n_o and n_e are lowered by the spontaneous polarization P_S through the quadratic electrooptic effect. As discussed above, the proton-exchange reduces P_S in the exchanged region. This causes an increase of n_o and n_e in the exchanged layer given by:

$$\Delta n_o^P = \frac{1}{2} n_o^3 g_{13} (P_{S,0}^2 - P_{S,PE}^2)$$

$$\Delta n_e^P = \frac{1}{2} n_e^3 g_{33} (P_{S,0}^2 - P_{S,PE}^2) \qquad (2)$$

$P_{S,0}$ and $P_{S,PE}$ are the spontaneous polarizations in the bulk and the exchanged layer, respectively. According to Di Domenico and Wemple, the values of the quadratic electrooptic coefficients

g_{13} and g_{33} are approximately the same for all oxygen octahedral ferroelectrical materials. The values of g_{13} and g_{33}, derived from the coefficients given for a cubic perovskite lattice in Ref.32, are 0.02 and 0.09 m^4C^{-2}, respectively.

According to Sec.VI.A, $P_{S,PE} = 0$ in an as-exchanged waveguide. With g_{13} and g_{33} from Ref.32, Eq.(2) gives the following values for the index increase due to the reduction of P_S:

$\Delta n_e^P = +0.12$, $\Delta n_o^P = +0.03$ for $LiTaO_3$,

and

$\Delta n_e^P = +0.24$, $\Delta n_o^P = +0.06$ for $LiNbO_3$.

(ii) The proton-exchange process in $LiTaO_3$ and $LiNbO_3$ can be expressed as,

$$(Li_2O)(M_2O_5) + x\,H_2O \leftrightarrow (Li_2O)_{(1-x)}(H_2O)_x(M_2O_5) + x\,Li_2O, \tag{3}$$

where M is Ta or Nb.

The Clausius-Mossotti equation expresses a relation between the average refractive index $n = (n_o^2 n_e)^{1/3}$, the molar polarization α_M, and the molar volume V_M:

$$(n^2 - 1)/(n^2 + 2) = \alpha_M / V_M \tag{4}$$

Differentiation of Eq.(4) with respect to α_M gives an expression for the change of the refractive index due to a difference in α_M for Li_2O and H_2O:

$$\Delta n^{\alpha} = (n^2 + 2)^2 x(\alpha_M(H_2O) - \alpha_M(Li_2O))/12nV_M \tag{5}$$

With the isotropic molar polarizabilities for Li_2O and H_2O used in Ref.13, $\alpha_M(Li_2O) = 5.2\ cm^3$ and $\alpha_M(H_2O) = 3.7\ cm^3$, and with the exchange factor $x = 0.8$ after the proton exchange we obtain:

$\Delta n^{\alpha} = -0.066$ for $LiTaO_3$,

and

$\Delta n^{\alpha} = -0.070$ for $LiNbO_3$.

(iii) The increase of the c lattice parameter after proton exchange results in an increase of the molar volume V_M and thus a dilution of the refractive index. Differentiating Eq.(4) with respect to V_M we obtain

$$\Delta n^{V} = (n^2+2)(n^2-1)(V_{M,PE} - V_M)/6V_M \qquad (6)$$

where $V_{M,PE}$ is the molar volume for proton-exchanged $LiNbO_3$ or $LiTaO_3$. Neglecting small changes of the a lattice parameter, $\Delta c/c = 0.6$ % for $LiTaO_3$ and 0.4 % for $LiNbO_3$ give:

$\Delta n^{V} = -0.012$ for $LiTaO_3$,

and

$\Delta n^{V} = -0.009$ for $LiNbO_3$.

(iv) We assume that the deformation along the c axis is free so that the stress component $\sigma_z = 0$, and that the deformation in the xy-plane plane is uniform, $\varepsilon_x = \varepsilon_y = (a-a')/a'$. The primed cell parameter refer to the cell parameter of a powder with the same composition as the exchanged layer where the deformations are free in all directions. The index change due to the photoelastic effect may then be written,

$$\Delta n_o^{\varepsilon} = -\frac{1}{2} n_o^3 (p_{11} + p_{12} + k p_{13}) \varepsilon_x$$

(7)

$$\Delta n_e^{\varepsilon} = -\frac{1}{2} n_e^3 (2 p_{31} + k p_{33}) \varepsilon_x$$

where p_{ij} are elastooptic coefficients. The constant k = -2 C_{13}/C_{33} ≈ -0.3 for both $LiTaO_3$ and $LiNbO_3$, with the stiffness constants C_{13} and C_{33} given in Ref.34.

The free-expansion values of the lattice parameters of $Li_{(1-x)}H_xTaO_3$ have to the best of our knowledge not been measured. However, the change of the lattice parameters in $Li_{(1-x)}H_xNbO_3$ powder have been determined by Rice and Jackel [14,35]. They found that for the room-temperature equilibrium β phase, the *a* parameter decreases from 5.172 Å for x = 0.56 back to approximately the α-phase value of 5.148 for x = 0.75. As $\Delta a/a$ due to proton exchange is very small in *z*-cut single-crystal samples, this suggests that ε_x should be approximately zero in as-exchanged samples with x = 0.8. However, to establish that the photoelastic effect is of minor importance, we calculate index changes assuming a free-expansion value a' = 5.172 Å, which gives ε_x = - 0.5 %. With elastooptic coefficients from Ref.36 and 37 we obtain the following maximum elastooptic index changes:

Δn_e^{ε} = + 0.005, Δn_o^{ε} = + 0.0008 for $LiTaO_3$,

and

Δn_e^{ε} = + 0.008, Δn_o^{ε} = + 0.0003 for $LiNbO_3$.

Neglecting possible small photoelastic index changes, we can add the different contributions considered above to obtain the total index changes:

$\Delta n_e = + 0.04$, $\Delta n_o = - 0.05$ for $LiTaO_3$,

and

$\Delta n_e = + 0.16$, $\Delta n_o = - 0.02$ for $LiNbO_3$.

These values may be compared to the experimentally determined values:

$\Delta n_e = + 0.01$, $\Delta n_o = - 0.03$ [4] for $LiTaO_3$,

and

$\Delta n_e = + 0.12$, $\Delta n_o = - 0.04$ [38] for $LiNbO_3$

The discrepancy between the calculated values and the experimentally determined ones stresses the semi-quantitative nature of the model. However, the estimates are of the right order of magnitude and the model does explain why Δn_e is ten times larger in $LiNbO_3$ than in $LiTaO_3$: In $LiTaO_3$ the difference between the positive contribution from the quadratic electrooptic effect and the negative contributions, in particular from the reduced polarizability due to the $H_2O \leftrightarrow Li_2O$ substitution, is relatively small (~ 0.04). In $LiNbO_3$, which has a larger P_S, the quadratic electrooptic effect becomes more significant and the difference between the positive and negative contributions is rather large (~ 0.16).

One reason for the semi-quantitative character of the result is the use of an isotropic model for calculation of the contribution Δn^{α} due to different polarizabilities for oxygen-bonded lithium and hydrogen in the crystal. As implied by calculations discussed in the next section, a more accurate model should consider the anisotropy of the polarizabilities. Another reason is the uncertainty in the values for the quadratic electrooptic coefficients estimated in Ref.32.

C. Annealed waveguides

We now examine whether the discussed index model can explain the observed increase of n_e in $LiTaO_3$ waveguides in the initial stage of the annealing (*cf.* Fig.3) and why this index increase is usually not observed in $LiNbO_3$ waveguides. The increase of n_e during the first hour of annealing, as calculated from the effective indices shown in Fig.3, is approximately 0.01. During this annealing the *c* lattice parameter decreases about 0.3 % (*cf.* Fig.5) and a comparison with data presented in Ref.3 suggests that the exchange factor *x* in the exchanged layer of $Li_{(1-x)}H_xTaO_3$ decreases from approximately 0.8 to 0.6. Though the boundaries for the α and β phases are uncertain, the results of Ref.29 suggest that proton-exchanged $LiTaO_3$ remains in the β phase for, at least, $x > 0.4$. Thus, the waveguides considered here should mainly consist of β-phase $Li_{(1-x)}H_xTaO_3$ after 1 h annealing.

An, according to the model, obviously positive contribution to the index change comes from the back-substitution of lithium for hydrogen which occurs on annealing. According to Eq.(5) a decrease of *x* from 0.8 to 0.6 results in an increase of the refractive index $\delta(\Delta n^{\alpha}) = + 0.016$.

The volume effect due to the decrease of the *c* parameter gives a second positive contribution to the index change (Eq.(6)). The decrease of *c* of 0.3 % during the first hour of annealing leads to an increase of the refractive index $\delta(\Delta n^{V}) = + 0.006$ (0.26 %).

The index change resulting from a decrease of the *c* parameter was also calculated considering the anisotropic nature of the polarizabilities of the atoms in the crystal lattice. This was done using a point-dipole model implemented by Devarajan and Glazer [39]. The polarizabilities of the atoms in hexagonal $LiTaO_3$ were fitted to give $n_e = 2.192$ and $n_o = 2.16$ and the change of the refractive index due to a change of the *c* parameter was computed. In this model a 0.3 %

decrease of c results in an increase $\delta(\Delta n_e^V) = 0.009$ (0.41 %) and an increase $\delta(\Delta n_o^V) = 0.005$ (0.22 %). According to this model the anisotropy of the polarizabilities thus results in a proportionally larger increase of n_e than of n_o.

With the waveguide still in the β phase, the model proposed for $P_{S,PE}$ in Sec.VI.A implies that $P_{S,PE}$ remains equal to zero. Thus, $\delta(\Delta n_e^P) = 0$ during the first hour of annealing.

If we consider the index change due to the photoelastic effect to be negligible and add the contributions discussed above, we can conclude that in the first part of the annealing n_e increases approximately 0.02. Due to a smaller volume effect in $LiNbO_3$, the change of n_e of $LiNbO_3$ should be somewhat smaller than that of $LiTaO_3$. The estimated increase of the refractive index on annealing of $LiTaO_3$ is of the same order of magnitude as that experimentally observed, and also of the same magnitude as the total index increase. In $LiNbO_3$ on the other hand, the index change on annealing is an order of magnitude smaller than the total index increase. This may explain why an increase of n_e on annealing is generally not observed in $LiNbO_3$ waveguides. However, a recent study by Ziling *et al.* suggests that for very thick proton exchanged layers there are annealing parameters for which Δn_e increases with annealing also in $LiNbO_3$ [13].

For prolonged annealing more and more of the material is transformed to the α phase and $P_{S,PE}$ starts to increase. Through Eq.(2) this causes a decrease of n_e with further annealing (*cf.* Fig.3). With the expression for $P_{S,PE}$ of the α phase from Eq.(1), Eq.(2) gives that $\Delta n_e^P \propto 2x\text{-}x^2$. For small x this indicates an approximately linear relation between Δn_e^P and x. Since also Δn^α depends linearly on x (Eq.(5)), the model discussed here is consistent with the observation that for well-annealed waveguides the area under the refractive-index profile is constant for different annealing times [4,19,23,40], indicating a linear relation between Δn_e and the hydrogen concentration.

VII. SHORT-TERM INDEX INSTABILITY

We have observed that for certain processing parameters annealed proton-exchanged waveguides in $LiTaO_3$ suffer from a large index decrease the first few days after the annealing [4]. This index decrease can be as large as 0.01, *i.e.* of the same order of magnitude as the total index increase. The process is reversible so that if the waveguide is heated again the refractive index increases and the ageing process will recommence. In addition there is a smaller long-term index change which continues for months [4,5,6]. It has earlier been shown that proton-exchanged waveguides in $LiNbO_3$ suffer from refractive-index instabilities as-exchanged [41] but that they become stable after post-exchange annealing [42]. The index changes observed in as-exchanged waveguides have been suggested to be due to a metastable β phase of $Li_{(1-x)}H_xNbO_3$ [35]. It is possible that the phase diagram of $Li_{(1-x)}H_xTaO_3$ is sufficiently different from that of $Li_{(1-x)}H_xNbO_3$ to explain why index changes are observed even in annealed $LiTaO_3$ waveguides.

To investigate whether the large short-term index changes can be attributed to the relaxation of an unstable crystal phase we used HRXRD to characterize a sample (2 h proton exchange at 260°C and 4 h annealing at 400°C) during the first period of time after the annealing. The processing parameters used have been found to produce waveguides with a drastically decreasing refractive index [4]. The XRC of the 0 0 6 reflection was monitored as function of time after the annealing. No significant structural changes were observed and we did not see any noteworthy difference between the *+c* and *-c* faces. Though we cannot rule out the possibility that post-annealing phase transitions occur in a thin surface layer that is poorly probed using the 0 0 6 reflection, our measurements suggest that phase transitions do not cause the observed short-term index change. The smaller long-term change of the refractive index was not studied here.

In the foregoing study [4] we used $LiTaO_3$ wafers polished only on the -*c* face, and thus only waveguides fabricated on the -*c* face were investigated. This is the crystal face at which domain reversal may occur in $LiTaO_3$ following proton exchange and heat treatment [43]. Here we also studied waveguides fabricated on the +*c* face. Slab waveguides were formed in samples polished on both faces using the processing parameters specified in the previous paragraph. After the annealing, the waveguides on both faces were characterized using standard prism-coupling technique.

Figure 9 shows the effective index N_0 and N_1 as functions of time after the annealing. As expected from the previous study N_0 decreases abruptly in the waveguide on the -*c* face (Fig.9:diamonds). The waveguide on the +*c* face (Fig.9:stars) is different, it is fairly stable and directly after the annealing it has the same index profile as the waveguide on the -*c* face attains after relaxation for a few days. A different result was obtained with a waveguide fabricated by proton exchange at 260°C for 2 h followed by annealing at 350°C for 21 h. This processing produces a waveguide that is stable also on the -*c* face. The waveguide supports six TM modes with the same effective indices as those attained after relaxation of the waveguide annealed at 400°C, *i.e.* the two different annealing conditions produce waveguides with similar equilibrium index profiles and thus similar hydrogen-concentration profiles. A possible disparity between the waveguides annealed at different temperatures may be that ferroelectric domain reversal has occured in one of them but not in the other. Chemical etching in $HF:HNO_3$ does indeed reveal the presence of an approximately 1 μm thick domain-inverted layer at the -*c* face of the waveguide annealed at 400°C, whereas no such layer is observed in the sample annealed at 350°C.

The domain reversal at the -*c* face results in a tail-to-tail domain boundary between the bulk and the inverted layer. According to Poisson's equation the change-of-sign of P_S at the domain boundary acts as a source for a depolarizing electric field. It is possible that this field induces a refractive-index change through the electrooptic effect and that charge compensation at room

temperature reduces the internal electric field, thus causing a time-dependent decrease of the refractive index. This would explain why index changes are observed only at the -*c* face and only when domain inversion has occured. It also explains why this phenomenon has not been observed in $LiNbO_3$ waveguides. Domain reversal at temperatures used for annealing of proton-exchanged waveguides only occurs in $LiTaO_3$.

In the previous study [4], we reported that a large index change occurs in waveguides fabricated by proton exchange at 260°C for 5 h followed by annealing for 4 h at 400°C, but that the same proton exchange followed by annealing for just 1 h resulted in fairly stable waveguides. Though domain inversion should have occured in both cases the result may be explained if it is assumed that the electrooptic coefficient r_{33} is reduced in the diffused layer for just 1 h annealing. It is known that proton exchange degrades the electrooptic coefficient and that rather strong annealing is necessary to recover it [2]. This explanation is also supported by a recent study, mentioned in Sec. VI.A, which shows that the second-order nonlinear coefficient d_{33} in a waveguide initially exchanged for 5 h at 260°C is still strongly reduced after 1 h annealing at 400°C, but has more or less recovered after 4 h annealing [29].

The explanation proposed here for the observed index change can also explain the reversability of the process: If the waveguide is heated again P_S will decrease through the pyroelectric effect. To compensate for this the free charge which accumulated at the domain boundary at room temperature will diffuse out of that region. When the crystal is cooled to room temperature again P_S increases and the uncompensated discontinuity of P_S at the domain boundary results in a depolarizing field which through the electrooptic effect again causes a temporary index increase.

It should be added that the long-term instability which is observed also in *z*-cut waveguides in which no domain inversion has occured and in *x*-cut waveguides [5], cannot be explained by the model suggested here for the short-term instability. In that case it seems more likely that the instability is due to the presence of a metastable crystal phase.

VIII. CONCLUSIONS

Proton-exchanged waveguides in *z*-cut $LiTaO_3$ have been investigated. Observations made in the polarizing microscope together with IR absorption measurements indicates the formation of monoclinic phase $Li_{(1-x)}H_xTaO_3$ after proton exchange in pure pyrophosphoric acid. No such phase was observed in as-exchanged $LiNbO_3$. This monoclinic phase is transformed back to rhombohedral $Li_{(1-x)}H_xTaO_3$ in the very initial stage of the annealing. As a consequence this transformation cannot explain the previously found increase of the refractive index on annealing of $LiTaO_3$ waveguides.

High-resolution X-ray diffraction was used to examine the structural properties of $Li_{(1-x)}H_xTaO_3$. The *c* lattice parameter was found to be approximately 0.6 % larger in the as-exchanged region than in the bulk whereas the *a* lattice parameter was found to be slightly decreased (-0.05 %). The change of the *c* parameter is larger in $LiTaO_3$ than in $LiNbO_3$. On annealing the *c* parameter relaxes and in addition there appears a second diffraction peak in the rocking curve. This peak is attributed to α-phase $Li_{(1-x)}H_xTaO_3$. No other new phases or anomalous behaviour was observed which alone can explain the index increase in annealed $LiTaO_3$ waveguides.

A model for the increase of the refractive index is suggested where the main reason for the difference in index increase between as-exchanged waveguides in $LiTaO_3$ and $LiNbO_3$ is the larger value of the spontaneous polarization of $LiNbO_3$. The predicted increase of the index on annealing of $LiTaO_3$ is of the same order of magnitude as that experimentally observed, and also of the same magnitude as the total index increase. In $LiNbO_3$, the calculated index change on annealing is an order of magnitude smaller than the total index increase, which may explain why the increase of n_e on annealing is mostly observed only in $LiTaO_3$ waveguides.

The short-term post-annealing index decrease observed in a previous study is also examined and discussed. Experiments in this study show that the index change occurs only in waveguides

on the -*c* face. X-ray diffraction did not reveal any time-dependent structural changes which can explain the phenomenon. It is instead suggested that it is connected with the ferroelectric domain reversal: An internal electric field due to an initially uncompensated discontinuity of P_S at the domain boundary induces an index increase via the electrooptic effect. Charge compensation at room temperature then reduces the internal field, leading to a time-dependent decrease of the electrooptically induced refractive-index change.

ACKNOWLEDGEMENTS

The authors wish to thank Professor Harvey Rutt at Optoelectronics Research Centre, Southampton, for help with IR absorption measurements. This project was mainly financed by the Göran Gustafsson Foundation. Jonas Webjörn acknowledges support from the Swedish Institute.

REFERENCES

1. K. Yamamoto, K. Mizuuchi, Y. Kitaoka, and M. Kato, Appl. Phys. Lett. **62**, 2599 (1993).

2. T. Yuhara, K. Tada, and Y. Li, J. Appl. Phys. **71**, 3966 (1992).

3. P. J. Matthews, A. R. Mickelson, and S. W. Novak, J. Appl. Phys. **72**, 2562 (1992).

4. H. Åhlfeldt, J. Webjörn, F. Laurell, and G. Arvidsson, J. Appl. Phys. **75**, 717 (1994).

5. P. J. Matthews, and A. R. Mickelson, J. Appl. Phys. **71**, 5310 (1992).

6. H. Åhlfeldt and F. Laurell, in *Compact Blue-Green Lasers*, 1994 Technical Digest Series, Vol. 1 (Optical Society of America, Washington, DC, 1994), pp. 19 - 21.

7. N. V. Khaklova, and N. S. Dombrovskaya, Russian J. Inorg. Chem. **4**, 416 (1959).

8. V. A. Ganshin, and Y. N. Korkishko, Phys. Status Solidi (A) **119**, 11 (1990).

9. I. Savatinova, M. Kuneva, Z. Levi, V. Atuchin, K. Ziling, and M. Armenise, Proc. SPIE **1374**, 37 (1990).

10. A. Loni, G. Hay, R. M. De La Rue, and J. M. Winfield, IEEE J. Lightwave Technol. **LT-7**, 911 (1989).

11. J. L. Jackel and C. E. Rice, Ferroelectrics **38**, 801 (1981).

12. R. Richter, T. Bremer, P. Hertel, and E. Krätzig, Phys. Status Solidi (A) **114**, 765 (1989).

13. C. Ziling, L. Pokrovskii, N. Terpugov, I. Savatinova, M. Kuneva, S. Tonchev, M. N. Armenise, and V. M. N. Passaro, J. Appl. Phys. **73**, 3125 (1993).

14. C. E. Rice, J. Solid State Chem. **64**, 188 (1986).

15. V. A. Ganshin and Yu. N. Korkishko, J. Opt. Commun. **13**, 2 (1992).

16. C. Canali, A. Camera, G. Della Mea, P. Mazzoldi, S. M. Al Shukri, A. C. G. Nutt, and R. M. De La Rue, J. Appl. Phys. **59**, 2643 (1986).

17. M. Ito and K. Kawamoto, Jpn. J. Appl. Phys. **31**, 3882 (1992).

18. M. Minakata, K. Kumagai, and S. Kawakami, Appl. Phys. Lett. **49**, 992 (1986).

19. M. M. Howerton, W. K. Burns, P. R. Skeath, and A. S. Greenblatt, J. Quantum Electron. **27**, 593 (1991).

20. K. Sugii, M. Fukuma, and H. Iwasaki, J. Materials Science **13**, 523 (1978).

21. W. Hou, W. Hua, Y. Zhang, and H. Tan, Electron. Lett. **27** 755 (1991).

22. E. Y. B. Pun, W. X. Hou, Y. T. Chow, and P. S. Chung, Electron. Lett. **29**, 1453 (1993).

23. C. C. Ziling, V. V. Atuchin, I. Savatinova, and M. Kuneva, Internat. J. Optoelectron. **7**, 519 (1992).

24. I. Calimbel, J. Appl. Phys. **40**, 1690 (1969).

25. R. A. Becker, Appl. Phys. Lett. **43**, 131 (1983).

26. F. Laurell, M. G. Roelofs, and H. Hsiung, Appl. Phys. Lett. **60**, 301 (1992).

27. M. L. Bortz, L. A. Eyres, and M. M. Fejer, Appl. Phys. Lett. **62**, 2012 (1993).

28. H. Åhlfeldt, F. Laurell, and G. Arvidsson, Electron. Lett. **29**, 819 (1993).

29. H. Åhlfeldt, J. Appl. Phys., tentatively 15 September 1994.

30. B. F. Levine, Phys. Rev. **B 10**, 1655 (1974).

31. I. Savatinova, S. Tonchev, M. Kuneva, and E. Liarokapis, Appl. Phys. A **58**, 481 (1994).

32. M. Di Domenico and S. H. Wemple, J. Appl. Phys. **40**, 720 (1969).

33. J. Webjörn, IEEE J. Lightwave Technol. **LT-11**, 589 (1993).

34. R. T. Smith and F. S. Welsh, J. Appl. Phys. **42**, 2219 (1971).

35. C. E. Rice, and J. L. Jackel, Mat. Res. Bull. **19**, 591 (1984).

36. L. P. Avakyants, D. F. Kiselev, and N. N. Shchitov, Sov. Phys. Solid State **18**, 899 (1976).

37. L. P. Avakyants, D. F. Kiselev, and N. N. Shchitov, Sov. Phys. Solid State **18**, 1242 (1976).

38. M. De Micheli, J. Botineau, F. Sibillot, and D. B. Ostrowsky, Opt. Commun. **42**, 101 (1982).

39. V. Devarajan and A. M. Glazer, Acta. Cryst. A **42**, 560 (1986).

40. J. Nikolopoulos and G. L. Yip, IEEE J. Lightwave Technol. **LT-9**, 864 (1991).

41. A. Yi-Yan, Appl. Phys. Lett. **42**, 633 (1983).

42. J. L. Jackel and C. E. Rice, Proc. SPIE **460**, 43 (1984).

43. K. Nakamura and H. Shimizu, Appl. Phys. Lett. **56**, 1535 (1990).

FIGURE CAPTIONS

Fig.1 Micrograph of the as-exchanged *z* face of a $LiTaO_3$ sample viewed between crossed polarizers. The black regions correspond to biaxial domains extinguishing at the present angle of rotation of the sample.

Fig.2 Infrared transmission spectra for three *z*-cut samples initially exchanged for 5 h at 260°C; (a) as-exchanged, (b) annealed for 10 min at 300°C, and (c) annealed for 15 min at 350°C.

Fig.3 Effective indices (N_0 to N_6) versus root of annealing time for waveguides initially exchanged for 5 h at 260°C and subsequently annealed at 350°C. The effective indices were measured 5 months after the annealing (From Ref.4).

Fig.4 X-ray rocking curves for (a) 0 0 6 and (b) 0 0 12 reflections from *z*-cut samples (A-F) initially exchanged for 5 h at 260°C. Sample A is as-exchanged, the others have been annealed at 350°C for 5 min (B), 10 min (C), 20 min (D), 1 h (E), and 4 h (F).

Fig.5 $\Delta c/c$ versus root of annealing time. The squares represent the large low-angle peak and the diamonds the small high-angle peak.

Fig.6 $\Delta c/c$ versus $KHSO_4$ concentration in the melt for samples exchanged in sulphate-salt melts.

Fig.7 Typical XRC for the 0 0 6 reflection from a *z*-cut $LiNbO_3$ sample exchanged for 5 h at 260°C. The largest satellite peak corresponds to $\Delta c/c = 0.32$ %.

Fig.8 A two-dimensional diffraction space map (ω *vs.* ω-2θ) of the 5 0 8 reflection for a sample exchanged for 5 h at 260°C and annealed for 10 min at 350°C. The peak in the top-right corner is from the substrate and the one in the bottom-left corner is from the proton-exchanged layer.

Fig.9 Effective indices N_0 and N_1 as function of time after the annealing for a waveguide formed at the *-c* (diamonds) and *+c* (stars) face. Annealing was carried out at 400°C. The last points show the effective indices 10 min after an additional heat treatment (10 min at 150°C).

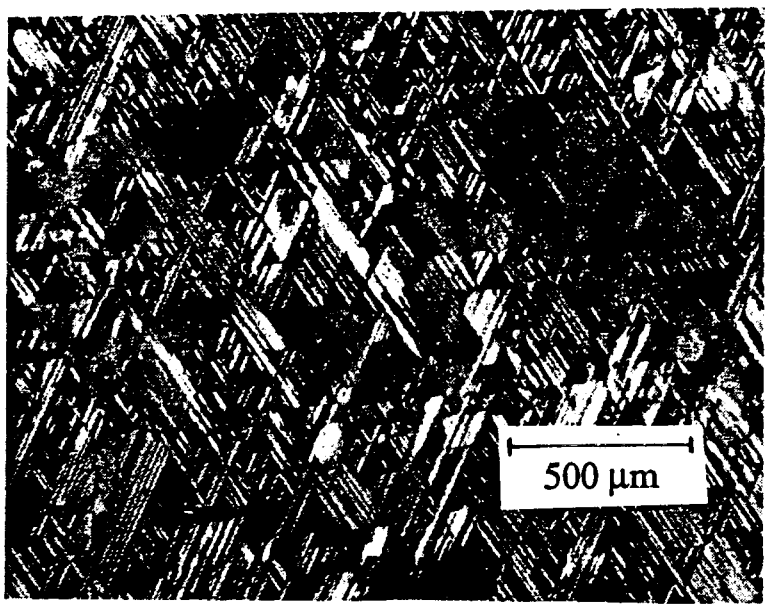

Fig. 1

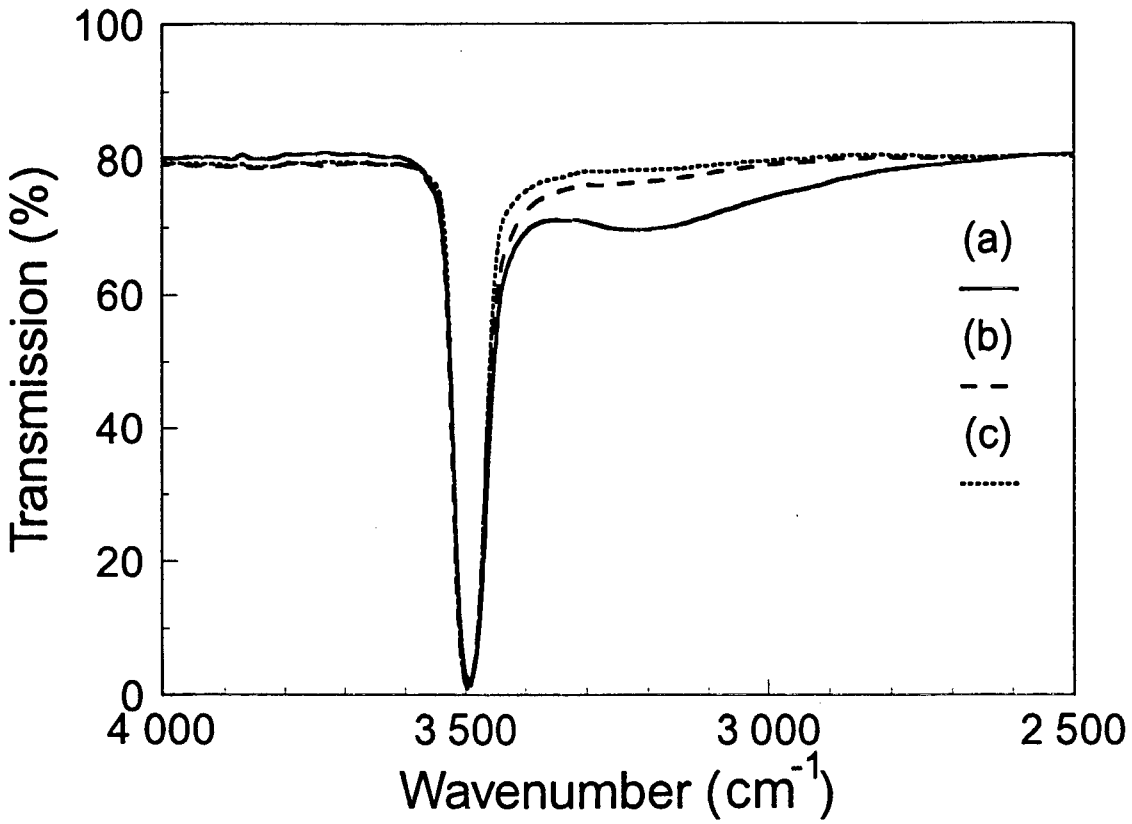
100
80
60
40
20
0
Transmission (%)
4 000
3 500
3 000
2 500
Wavenumber (cm-1)
(a)
(b)
(c)

Fig. 2

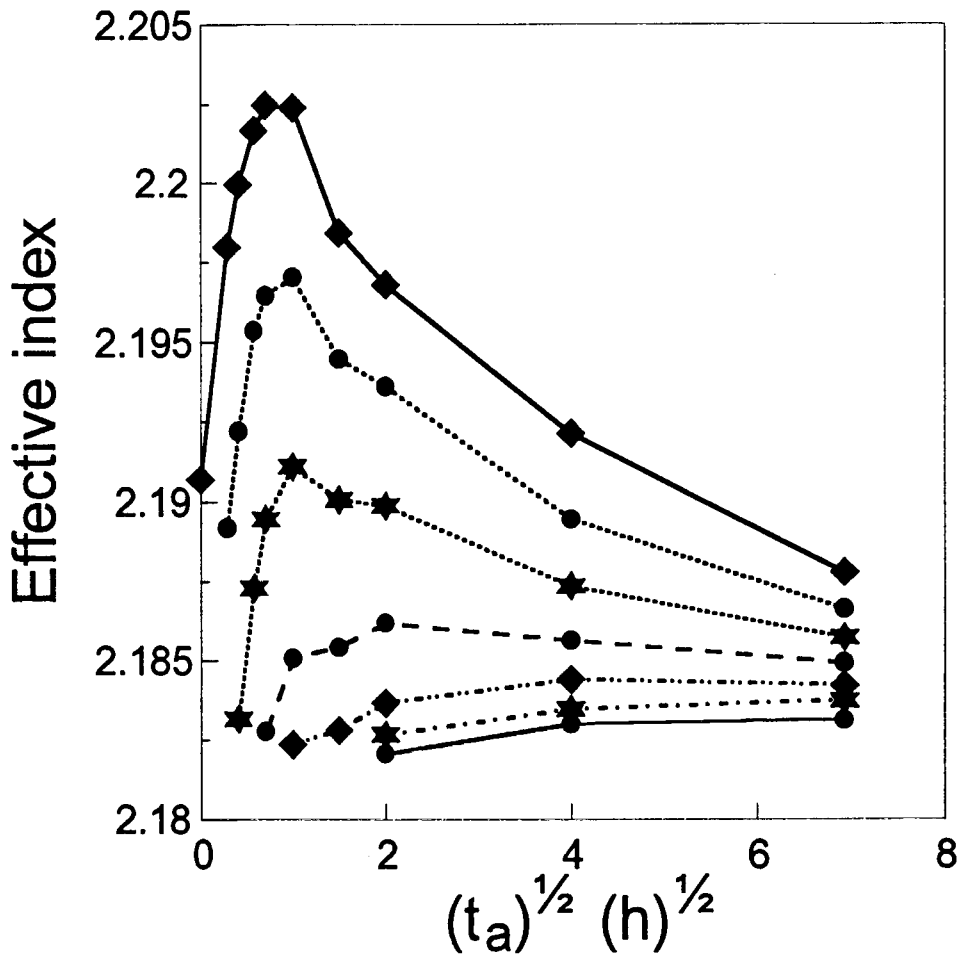

Fig. 3.

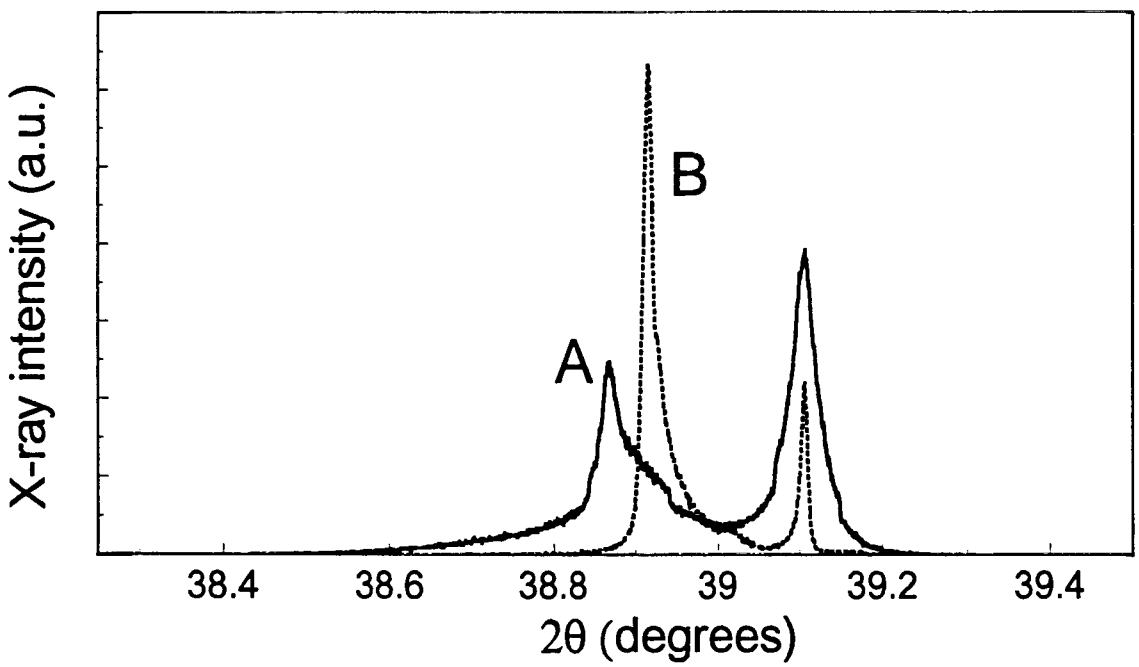

Fig. 4(a)

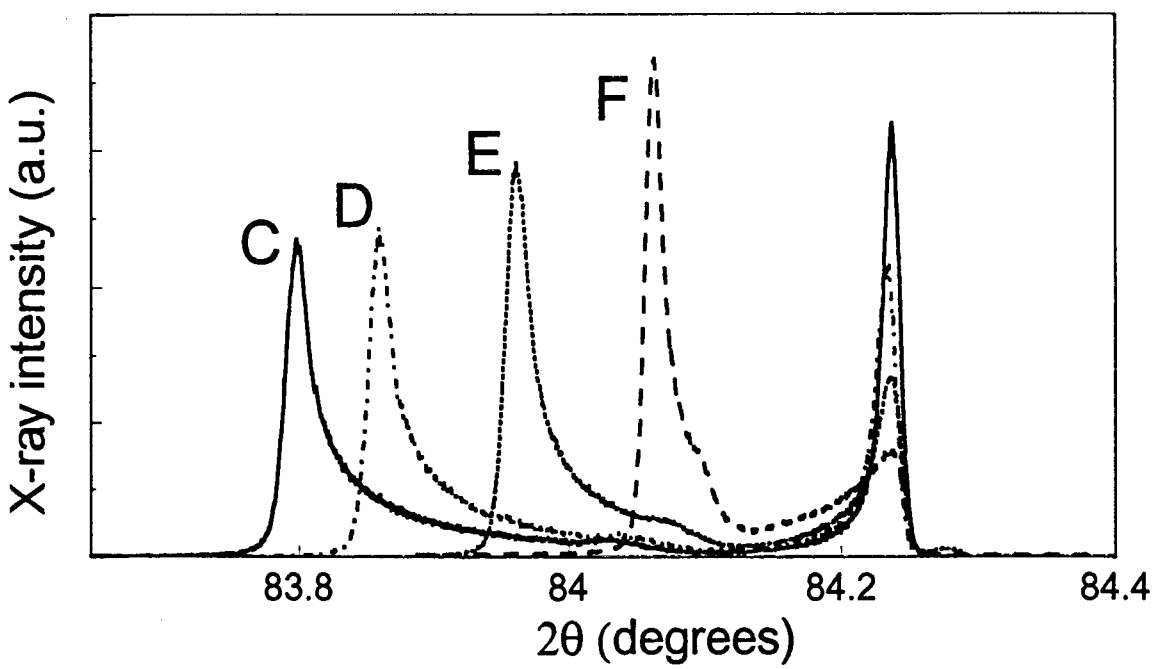

Fig. 4 (b)

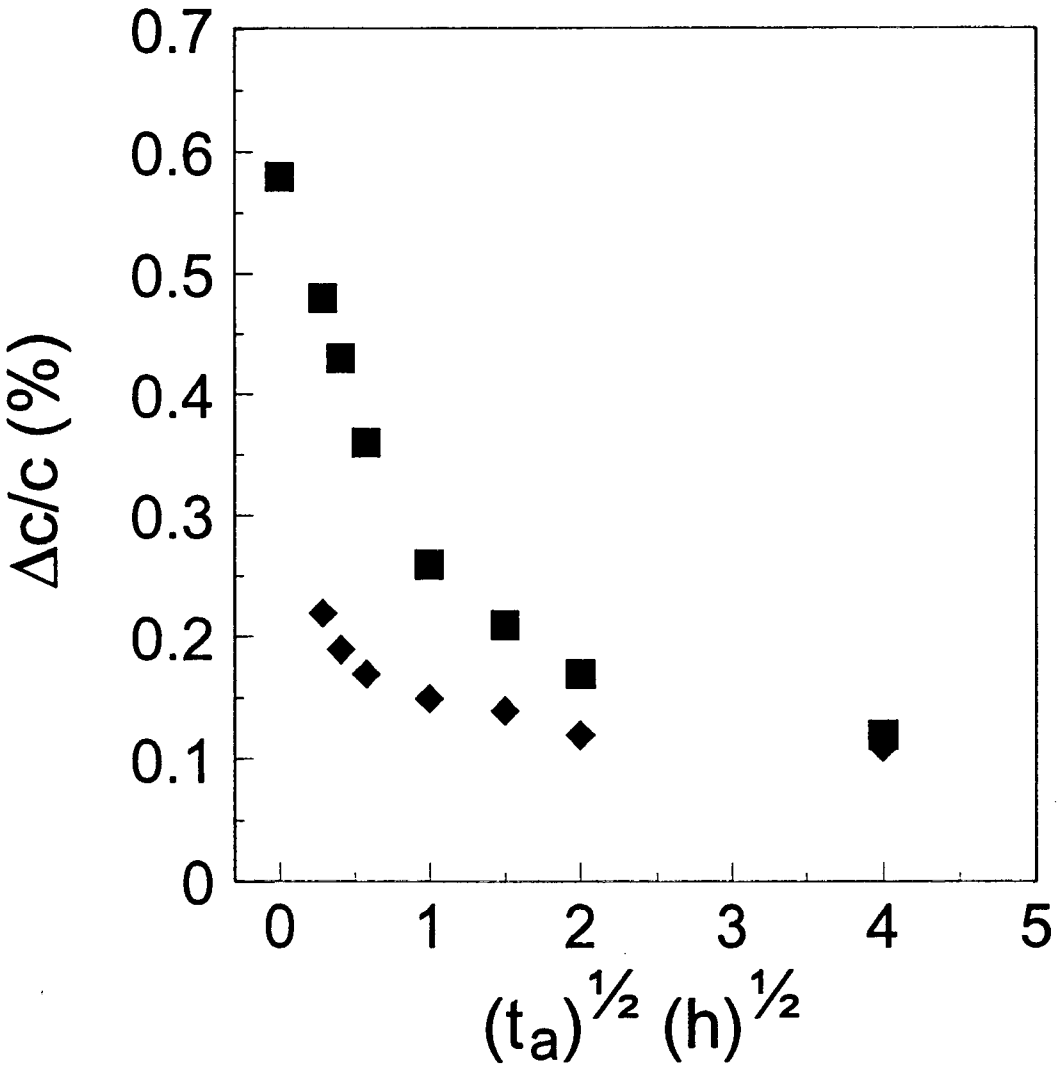

Fig. 5

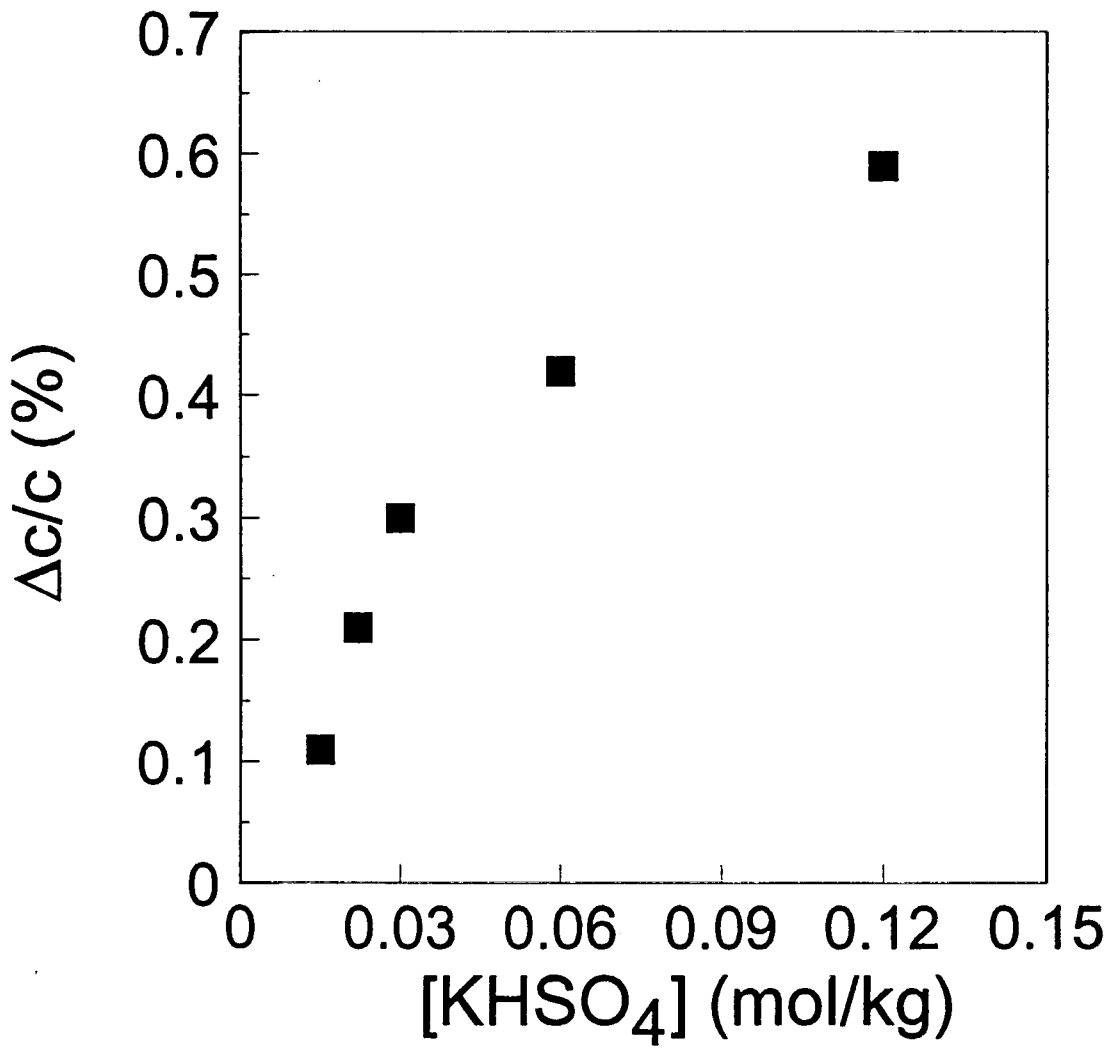

Fig. 6

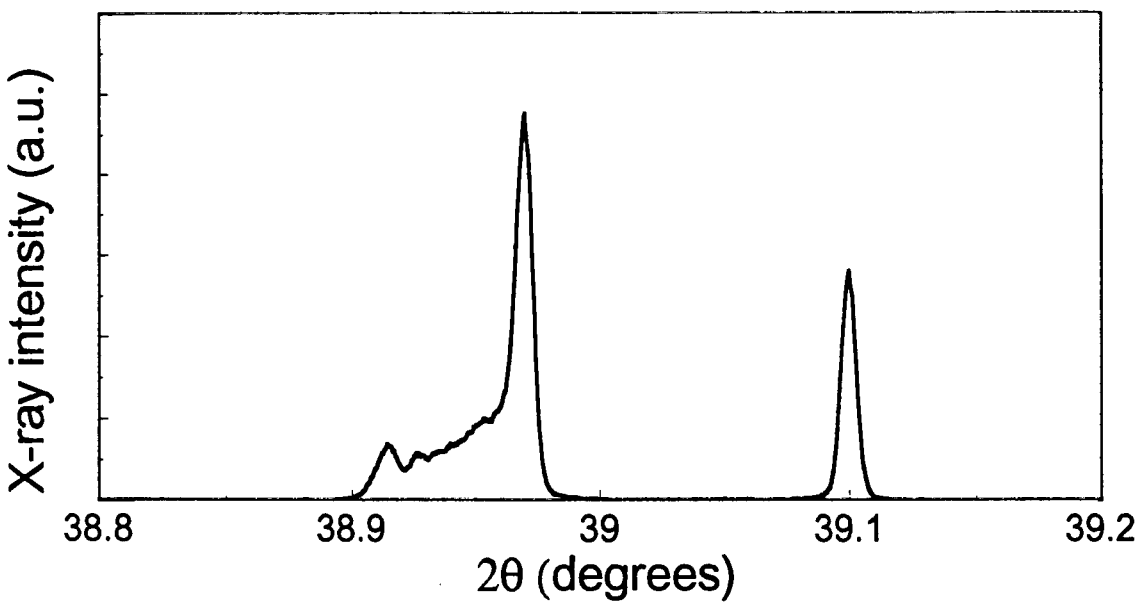

Fig. 7

Fig. 8

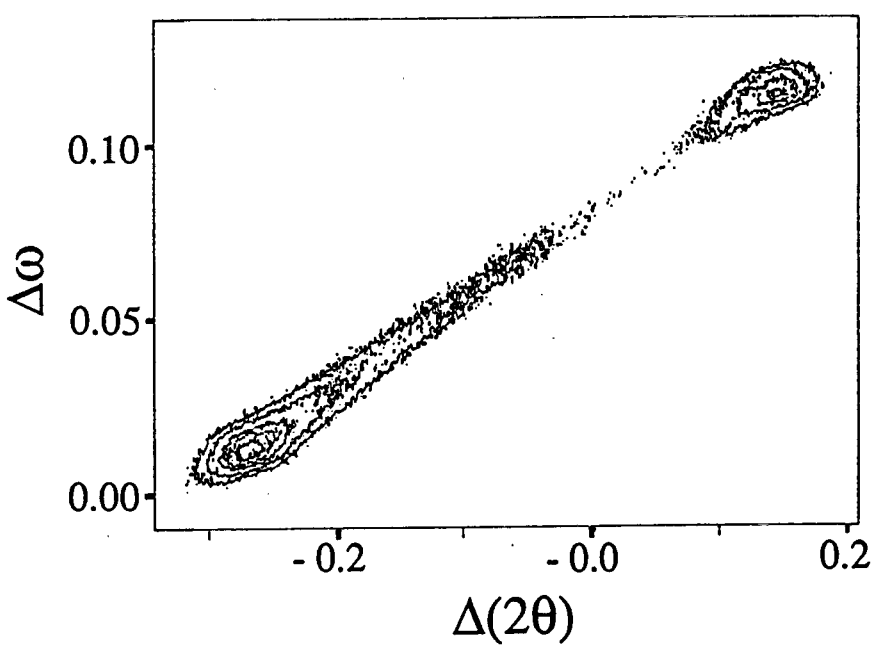

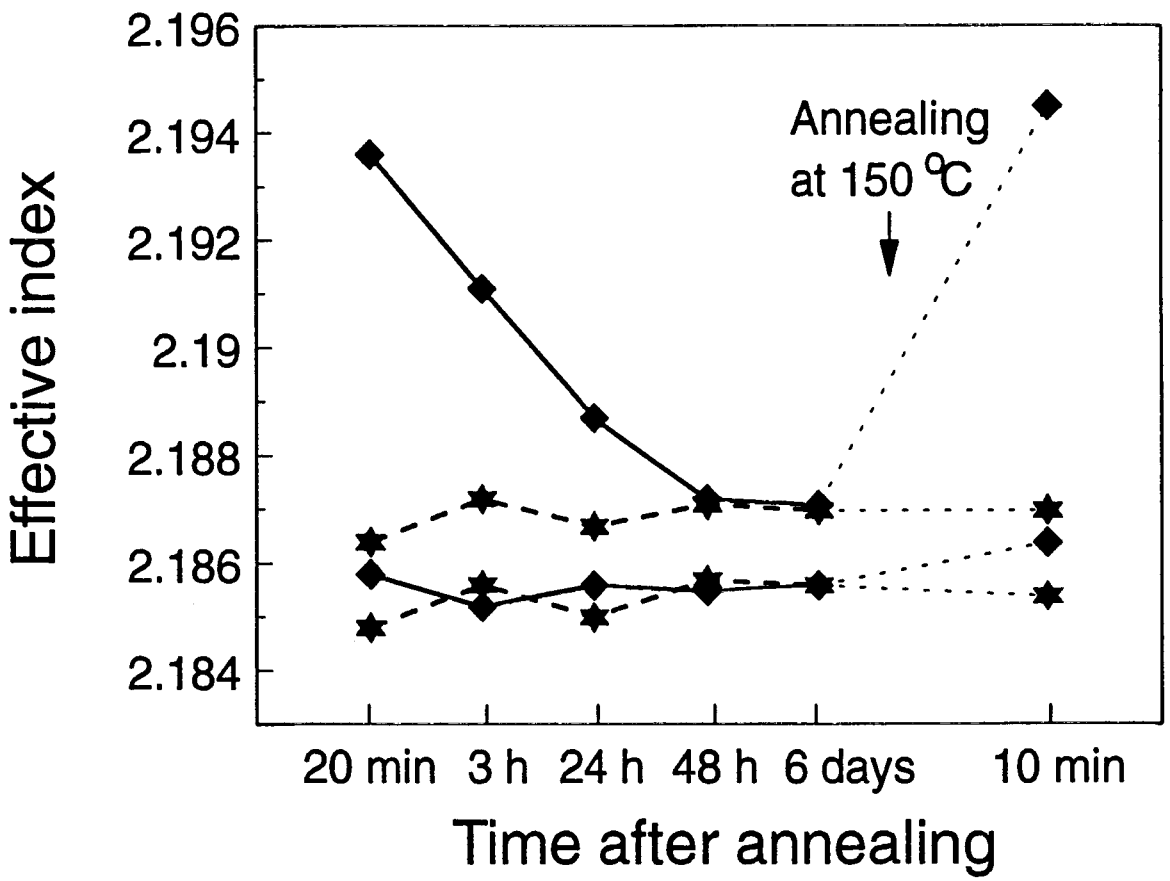
2.196
2.194
2.192
2.19
2.188
2.186
2.184
Effective index
Annealing
at 150 °C
20 min
3 h
24 h
48 h
6 days
10 min
Time after annealing

Fig. 9